

High-energy colliders and the rise of the standard model

Terry Wyatt¹

Over the past quarter of a century, experiments at high-energy particle colliders have established the standard model as the precise theory of particle interactions up to the 100 GeV scale. A series of important experimental discoveries and measurements have filled in most of the missing pieces and tested the predictions of the standard model with great precision.

The standard model of particle physics describes the Universe as being composed of a rather small number of different types of elementary particle (see page 270) that interact in a small number of well-defined different ways.

Interactions among the elementary particles are represented by Feynman diagrams such as those in Fig. 1a. These show the annihilation of an electron–positron (e^+e^-) pair to produce a fermion–antifermion pair (such as a quark–antiquark or lepton–antilepton pair), and such interactions are examples of the ‘electroweak’ interaction, which is propagated by the photon, W^\pm and Z bosons. All of the fermions participate in the electroweak interaction; certain ‘self-interactions’ among the photon, W and Z bosons may also take place.

Quarks, but not leptons, also participate in the strong interaction, which is propagated by gluons and described by the theory of quantum chromodynamics (QCD). Collectively, quarks and gluons are referred to as ‘partons’. Quarks may carry one of three ‘colours’, which in the

strong interaction are the analogue of charge; antiquarks carry the equivalent anticoulour. A particular feature of the strong interaction is that coloured quarks cannot exist as free particles for more than about 10^{-24} s. The particles we observe in our detectors are hadrons — collections of quarks and/or antiquarks that have no net colour. There are two basic types of hadron: mesons contain a quark and an antiquark (of opposite colour); baryons contain three quarks (one of each colour). When a high-energy quark or gluon is produced, it is observed as a collimated ‘jet’ of hadrons.

The Higgs mechanism is introduced into the standard model to allow elementary particles to have non-zero masses, through their interaction with the Higgs field, while maintaining the gauge invariance of the model. A consequence of including the Higgs mechanism is that a massive, spin-zero Higgs boson is also predicted to exist.

If the mathematical structure of the standard model is taken as a given (although, of course, it represents a considerable amount of empirical input!), then all particle couplings are predicted in terms of a relatively small number of ‘free’ parameters that must be determined by experiments. For example, the strong interaction is determined by the value of a single coupling constant, denoted α_s . In the electroweak sector, the physically observed photon and Z boson arise from a linear superposition of two hypothetical particles: the W^0 , the electrically neutral partner of the W^\pm , and another neutral boson, B^0 (of the so-called ‘hypercharge’ interaction). A rotation angle is defined between the W^0/B^0 and Z /photon, known as the electroweak mixing angle, θ_w , which describes the relative strengths of the electromagnetic and weak interaction. The interactions of the photon, Z and W are then determined by three free parameters. Logically, these can be thought of as the coupling constants of the weak and hypercharge interactions and the electroweak mixing angle. The masses of the W and Z bosons can also be predicted in terms of these parameters (with the photon and gluon required to be massless by gauge invariance). The masses of the 12 fermions and the Higgs boson are not predicted and thus represent additional free parameters that must be determined by experiment.

A particular feature of the electroweak interactions is that the couplings of the fermions to the W and Z depend on their handedness or helicity. The W^\pm couples only to left-handed (negative-helicity) fermions and right-handed (positive-helicity) antifermions. The Z couples to both left- and right-handed fermions, but with a different coupling constant in each case.

In simple terms, the basic aims of particle physics are to find direct experimental evidence for each of the elementary particles and to make as precise as possible measurements of their various properties

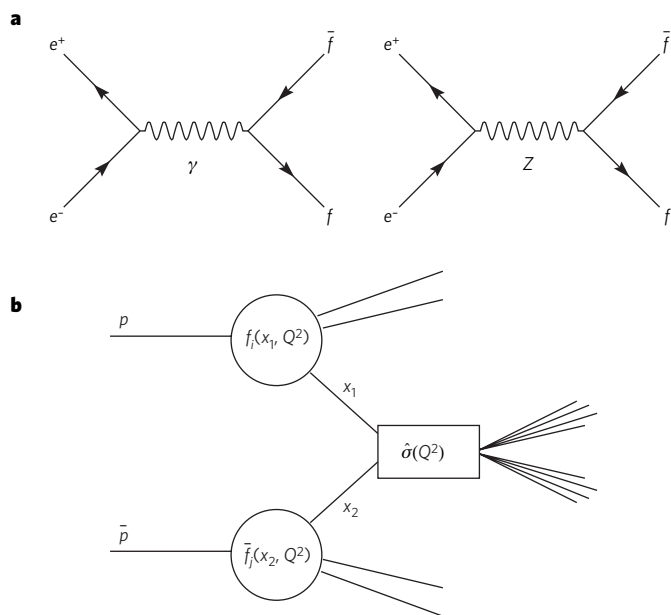


Figure 1 | Particle interactions. a, The lowest-order Feynman diagrams for the process $e^+e^- \rightarrow f\bar{f}$, where f is any elementary fermion (quark or lepton). **b**, Schematic view of a high-energy $p\bar{p}$ collision. Part b reproduced, with permission, from ref. 16.

¹Particle Physics Group, School of Physics and Astronomy, University of Manchester, Manchester, UK.

(masses, coupling strengths and so on). Because the number of different experimental measurements that can be made is much larger than the number of free parameters in the standard model, we are dealing with an ‘over-constrained’ system. That is, our experimental measurements not only determine the values of the free parameters of the standard model, they also provide stringent tests of the consistency of the model’s predictions.

Electrons versus protons

For more than a quarter of a century, the high-energy frontier of particle physics has been dominated by experiments performed at particle–antiparticle colliders. In these accelerators, beams of electrons and positrons, or protons (*p*) and antiprotons (*p̄*), travel with equal and opposite momenta and collide head-on in the centre of the particle detectors.

Experiments at electron colliders have several advantages over those at proton colliders, which stem from the fact that electrons are elementary particles. When an *e⁺e⁻* pair annihilates, the initial state is well defined and, if the pair collide at equal and opposite momentum, the centre-of-mass energy of the system (*E_{cm}*) is equal to the sum of the beam energies. *E_{cm}* is the energy available to produce the final-state particles.

Electrons participate only in the electroweak interaction. This means that the total *e⁺e⁻* annihilation cross-section is small, so event rates in experiments are low, but essentially every annihilation event is ‘interesting’, and the observed events are relatively simple to analyse. Initial-state *bremsstrahlung* (radiation from the beam particles) can reduce the available centre-of-mass energy, but because this is a purely electromagnetic process it can be calculated with great precision, and it introduces no significant systematic uncertainties into the analysis of annihilation events.

The disadvantage of using electrons as beam particles is their small rest mass. When high-energy electrons are accelerated, they lose energy (producing synchrotron radiation), and that energy loss must be compensated by the machine’s accelerating cavities. The energy radiated by a charged particle in performing a circular orbit of radius, *R*, is proportional to γ^4/R , where γ is the ratio of the particle’s total energy to its rest mass, *m₀c²*. Even though the world’s largest particle accelerator, the Large Electron–Positron Collider (LEP), at CERN, had a circumference of 27 km, its maximum beam energy of around 104 GeV was limited by the fact that each particle radiated about 2 GeV per turn. By contrast, the large rest mass of the proton means that synchrotron energy loss is not a significant limiting factor for proton–antiproton colliders. For example, the world’s highest energy collider at present is the Tevatron proton–antiproton collider, at Fermilab (Batavia, Illinois), which, with

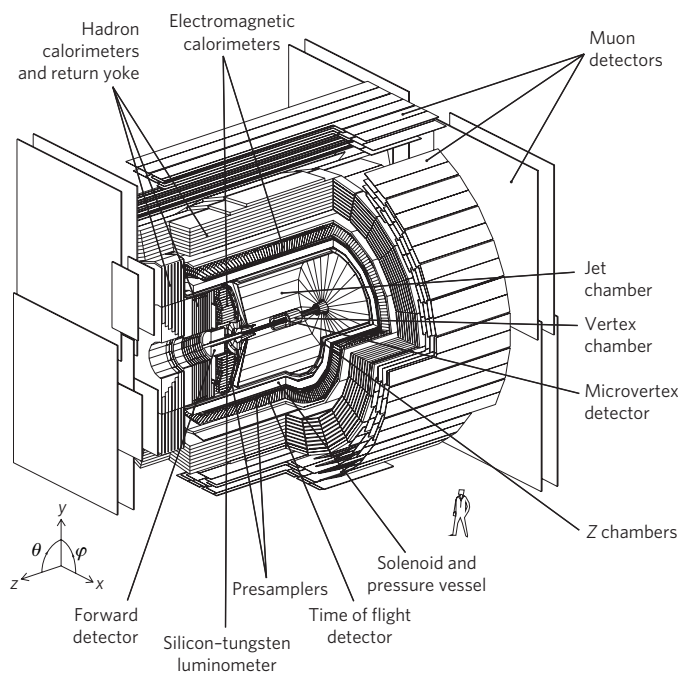


Figure 2 | The OPAL experiment at LEP. The typical, hermetic design of this detector comprises central track detectors inside a solenoid, calorimeters and — the outermost layers — muon detectors.

a circumference of only 6 km, achieves a beam energy of 1,000 GeV (or 1 TeV); the Large Hadron Collider (LHC), using two proton beams in the 27-km LEP tunnel, will achieve beam energies of 7 TeV.

Although the beam energies of proton colliders may be much higher, for experiments at these colliders there are a number of challenges that stem from the fact that protons and antiprotons are strongly interacting, composite particles. A high-energy proton–antiproton collision is shown schematically in Fig. 1b. The highest energy collisions take place between a valence quark from the proton and an antiquark from the antiproton. These colliding partons carry fractions *x₁* and *x₂* of the momentum of the incoming proton and antiproton, respectively. The energy, *Q*, in the parton–parton centre-of-mass frame is given by $Q^2 = x_1 x_2 E_{cm}^2$. The probability of a proton containing a parton of type *i* at the appropriate values of *x₁* and *Q²* is given by a ‘parton distribution function’ (PDF), *f_i(x₁, Q²)*. The cross-section for the parton–parton collision to produce a given

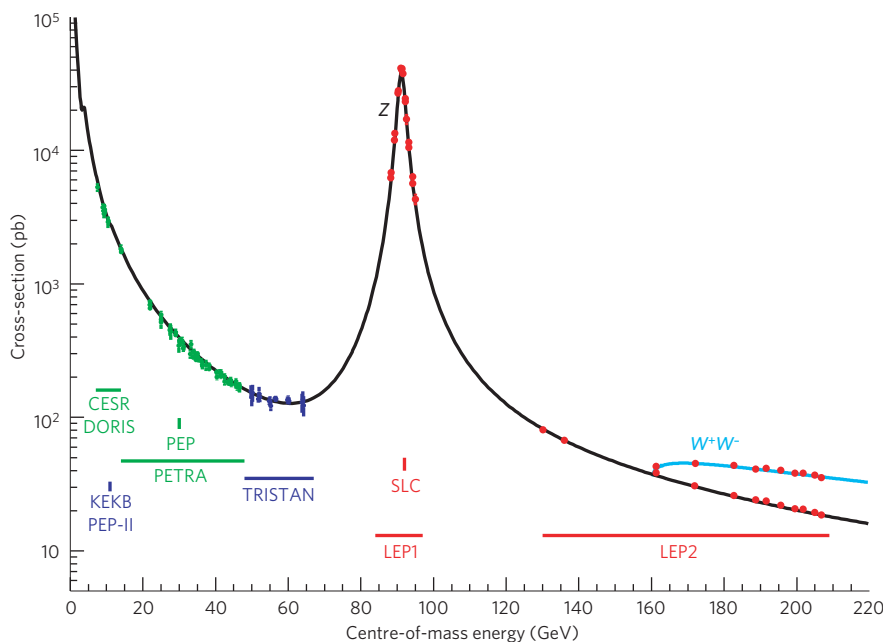


Figure 3 | The cross-section for *e⁺e⁻* annihilation to hadrons as a function of *E_{cm}*. The solid line is the prediction of the standard model, and the points are the experimental measurements. Also indicated are the energy ranges of various *e⁺e⁻* accelerators. (A cross-section of 1 pb = 10⁻⁴⁰ m².) Figure reproduced, with permission, from ref. 12.

final state is denoted by $\hat{\sigma}(Q^2)$. To determine the cross-section, σ , for the proton–antiproton collision to produce this final state, we have to sum over all possible combinations of incoming partons and integrate over the momentum fractions x_1 and x_2 :

$$\sigma = \sum_{ij=q,\bar{q},g} \int dx_1 dx_2 f_i(x_1, Q^2) \cdot \bar{f}_j(x_2, Q^2) \cdot \hat{\sigma}(Q^2)$$

Therefore, the proton and antiproton beams, at a fixed beam energy, can be thought of as broadband beams of partons.

The total cross-section for proton–antiproton collisions at high energy is huge, and the event rate is consequently large — at the Tevatron, for example, about 10 collisions take place each time the bunches of protons and antiprotons meet and cross each other in the circular machine. Such bunch crossings take place 1.7 million times each second. But most of these collisions are rather uninteresting, because they result from a low momentum transfer between the proton and antiproton. Interesting processes, such as those containing W or Z bosons, are produced at a much lower rate and can be difficult to observe above the huge background.

Furthermore, the PDFs cannot be calculated from first principles in QCD. They can, however, be fixed by experimental measurements. A great deal of information on PDFs has come from the H1 and ZEUS experiments at the HERA collider, at DESY (Hamburg). At HERA, 27.5-GeV beams of electrons or positrons collide with a 920-GeV beam of protons, to produce 320 GeV in the centre-of-mass frame. The electrons and positrons provide a clean (electroweak-interaction) probe of the

proton structure, and hence the PDFs, at these energies; the measured PDFs can then be extrapolated, using, for example, the so-called DGLAP evolution equations of QCD, to the much higher energies that are relevant at the Tevatron and the LHC.

A further complication is that the initial-state partons have a high probability of radiating gluons before they collide. To some extent, this can be compensated by tuning Monte Carlo simulations of the collisions to those events that include leptonically decaying W and Z bosons (in which there is no complication from the possibility of final-state gluon *bremsstrahlung*). Nevertheless, the uncertainties associated with the lack of precise predictions for initial-state gluon *bremsstrahlung* represent a significant source of systematic uncertainty in many analyses.

Proton and electron colliders are thus complementary: proton colliders offer the energy reach to make discoveries; electron colliders provide a cleaner experimental environment in which it is easier to make precise measurements.

Experiments at high-energy particle colliders typically share many common features, which are motivated by the requirements of the various measurements to be made. The basic aims are to detect with high efficiency each particle produced in the high-energy collision, to measure as accurately as possible its energy and momentum and to determine its particle type. No single detector type can achieve all of the above for all types of particle. Therefore, an experiment comprises a number of different detector systems, each of which has a specialized function. For example, at the centre of most experiments are detectors that measure the tracks produced by charged particles. Calorimeters are used for energy measurement, and muon systems are used for specific identification of those particles. An important feature of such detectors is their hermetic nature, which allows any apparent imbalance in the net transverse momentum of the visible particles to be ascribed to the production of weakly interacting particles, such as neutrinos. Fig. 2 shows, as an example, a cut-away view of the OPAL experiment at LEP, which is typical of detector design.

Discoveries and mounting evidence

By the late 1970s, the majority of the elementary fermions had been discovered. In particular, the discovery in the mid-1970s of the bottom quark and the tau lepton firmly established the existence of a third generation of fermions. However, there was only indirect evidence for the existence of two members of that generation: the top quark and the tau neutrino.

By contrast, among the elementary bosons only the photon had been observed directly as a physical particle. Although there was strong indirect evidence for the existence of the gluon, the first direct evidence came from the observations in 1979 by the JADE, Mark-J, TASSO and PLUTO experiments at the 30–35-GeV e^+e^- collider PETRA, at DESY. These experiments found events containing three hadronic jets, which correspond to the quark and antiquark produced in the e^+e^- collision, plus a gluon radiated from one of the quarks. The W and Z bosons were observed directly for the first time in 1983, by the UA1 and UA2 experiments^{1–4} at the 560–640-GeV Super Proton Synchrotron (SPS) proton–antiproton collider at CERN — a collider project that was conceived for the specific purpose of finding these particles and was rewarded with the 1984 Nobel Prize in Physics. The masses of the W and Z measured by the UA1 and UA2 experiments were found to be consistent with expectations, which was a beautiful confirmation of the standard model in electroweak interactions.

The scene was then set in 1989 for the 90-GeV e^+e^- colliders, LEP1 at CERN and SLC at the Stanford Linear Accelerator Center (SLAC; California). The ALEPH, DELPHI, L3 and OPAL experiments at LEP1 and the SLD experiment at the SLC performed measurements of Z production and decay that still today form the cornerstone of the precise tests of the electroweak standard model. Measurements of the Z mass elevated it to one of the most precisely known quantities within the standard model. Measurements of the total decay width of the Z (to all possible particle types) and the partial decay widths into each visible final state (that is, all final states except for $Z \rightarrow \nu\bar{\nu}$) allowed the number

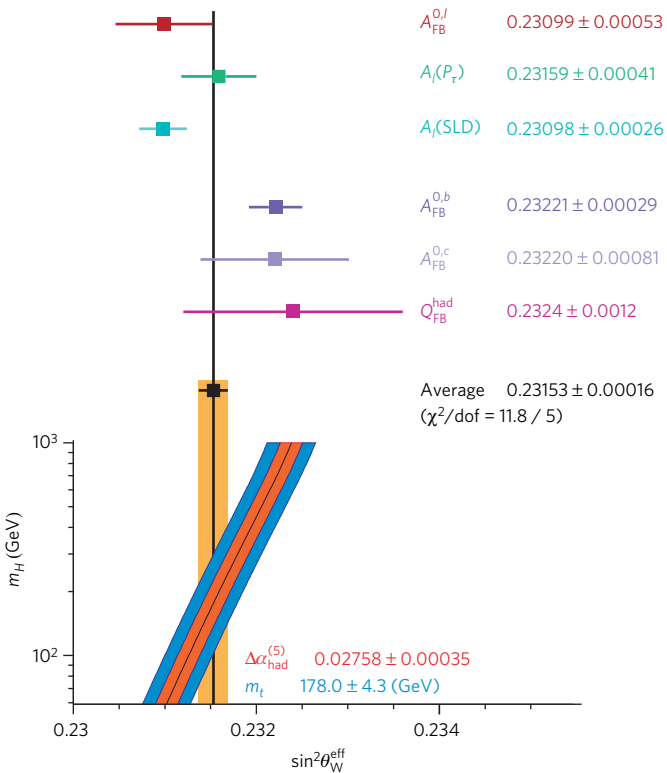


Figure 4 | Comparison of the effective electroweak mixing angle, $\sin^2\theta_W^{\text{eff}}$, derived from six classes of asymmetry measurements. These six classes are: A_{FB} , from leptonic final states at LEP; $A_l(P_\tau)$, derived from τ polarization measurements at LEP; $A_l(\text{SLD})$, derived from A_{lR} and from leptonic-final-state A_{lRFB} measurements at the SLC; and A_{FB} , from $b\bar{b}$ and $c\bar{c}$ final states at LEP. Q_{FB}^{had} is an average forward–backward charge asymmetry in hadronic events at LEP, without any attempt to distinguish individual quark flavours. Also shown is the standard-model prediction for $\sin^2\theta_W^{\text{eff}}$ as a function of m_H . The additional uncertainty of the standard-model prediction is parametric and dominated by the uncertainties in $\Delta\alpha_{\text{had}}^{(5)}(m_Z^2)$ (the correction for the effects of light-quark loops) and m_t , shown as bands. The total width of the band is the linear sum of these effects. Figure reproduced, with permission, from ref. 12. dof, degrees of freedom.

of light neutrino species to be fixed at three. This observation effectively confirmed the existence of the tau neutrino as a distinct physical particle within the three-generation standard model and ruled out the existence of a fourth generation of fermions, unless the neutrino from that generation has a mass greater than half that of the Z . (Direct observation of the tau neutrino was finally reported⁵ in 2001, in a different style of experiment using a proton beam directed at a fixed, tungsten target to produce neutrinos.)

Experimenters at all of the high-energy colliders since the days of PETRA had searched unsuccessfully for direct evidence for the existence of the top quark. These searches continued at 'Run I' of the 1.8 TeV Tevatron, which began in 1988. By 1994, the lower limit on the top quark mass from direct searches had reached^{6,7} about 130 GeV. By that time, there was also considerable indirect evidence for the existence of the top quark. For example, measurements of the electroweak couplings of the bottom quark were consistent with the hypothesis that it formed one half of a pair of third-generation quarks within the standard model. Furthermore, fits to the precise electroweak data from LEP1 and SLC gave self-consistent results within the standard model only if the effects of a top quark with a mass of between about 155 and 195 GeV were included.

The top quark was directly observed for the first time in 1995, by the CDF and DØ collaborations^{8,9} at the Tevatron. The first measurements gave its mass as 180 ± 15 GeV, consistent with the indirect determinations described above. This consistency represented a powerful confirmation of the electroweak standard model as an accurate picture of elementary particle physics.

In the second phase of the LEP programme, running between 1996 and 2000 with a vastly upgraded system of radio-frequency (RF) accelerating cavities, a maximum E_{cm} of nearly 209 GeV was reached. This allowed the production of W^+W^- pairs, enabling the ALEPH, DELPHI, L3 and OPAL experiments at LEP2 to measure the mass, m_W , and many other properties of the W boson.

In 2002, the second phase of running, Run II, began at the Tevatron. The accelerator complex was upgraded to deliver a slightly higher E_{cm} of 1.96 TeV and, more importantly, a greatly increased luminosity; the CDF and DØ detectors were also upgraded.

Now the most urgent question in particle physics (maybe in physics as a whole) is: where is the Higgs? Just as with the top quark, this question is being attacked on two fronts. Adding information from the direct measurements of the mass of the W boson and the top quark (from LEP2 and the Tevatron) to the precise electroweak measurements (from LEP1 and SLC) improves the precision with which the standard model can be tested. The overall fit gives self-consistent results only if the effects of a moderately light Higgs boson are included. Currently, a value for the Higgs mass of about 80 GeV is preferred, with an upper limit¹⁰, at a 95% confidence level, of 144 GeV; further improvements to the mass measurements from the Tevatron may narrow the confidence interval. Direct searches for the Higgs boson were performed at LEP. The best available direct lower limit¹¹ on the Higgs mass is currently 114 GeV (95% confidence level) from the search for $e^+e^- \rightarrow ZH$ at LEP2. This already excludes a large part of the confidence interval allowed by the standard-model fit. Direct searches for Higgs production are currently the subject of intense effort at the Tevatron, and sensitivity to masses beyond the LEP2 limit is expected in the near future.

Precise tests of the standard model

A central part of the particle physics programme over the past quarter of a century has been to test the consistency of the standard model through precise measurement of many of its parameters. Precise theoretical calculations, implemented through computer codes of high technical precision, and a careful assessment of residual theoretical uncertainties are also essential elements in efforts to confront the standard model using precise data.

Let us return to the simple process shown in Fig. 1a, the annihilation of an e^+e^- pair to produce a fermion–antifermion pair through an electroweak interaction mediated by the photon or Z boson. Particles that

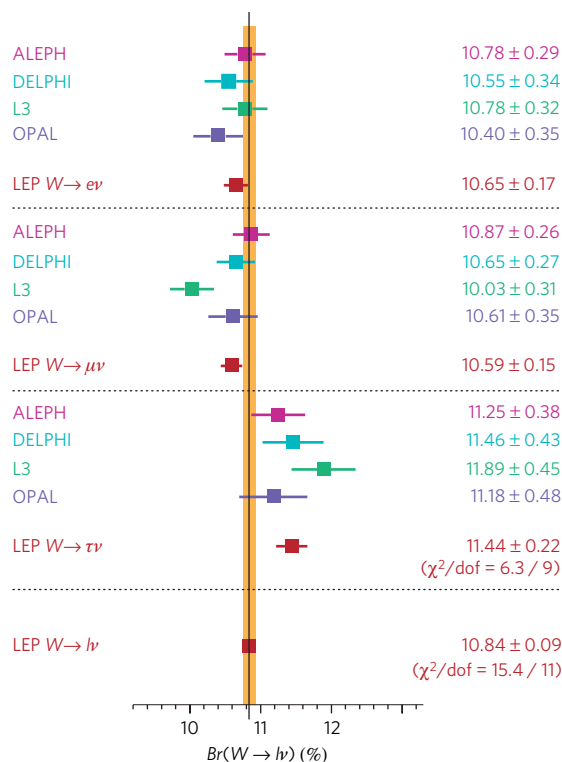


Figure 5 | Leptonic branching ratios. The measurements of the four LEP experiments of branching ratios for W decays to $e\nu$, $\mu\nu$ and $\tau\nu$ final states separately and for all lepton types combined. Figure reproduced, with permission, from ref. 14.

appear as internal lines in a Feynman diagram, such as the photon or Z in Fig. 1a, are 'virtual' particles — that is, they are not constrained to their 'physical' mass. However, the more virtual the particle becomes — the further away it is from its physical mass — the smaller the resultant amplitude for the process. Fig. 3 shows the cross-section for e^+e^- annihilation as a function of centre-of-mass energy, E_{cm} , based on data from several colliders including LEP and SLC. At low values of E_{cm} , the cross-section is dominated by the photon-exchange diagram (an exchanged Z would be highly virtual and the corresponding amplitude highly suppressed). With increasing E_{cm} , the cross-section falls as the exchanged photon becomes more and more virtual. At around 60 GeV, the amplitudes for photon and Z exchange are of comparable magnitude. As E_{cm} approaches the mass of the Z (91 GeV), the cross-section is dominated by the Z exchange diagram and reaches a peak, called the ' Z pole'.

The very large number of Z decays (around 20 million) collected by the experiments at LEP1 has allowed precise measurements of the couplings of the fermions to be made. The SLC delivered a much smaller number of Z decays (around 600,000) to the SLD experiment. However, the SLC delivered a longitudinally polarized e^- beam, which collided with an unpolarized e^+ beam, whereas at LEP both beams were unpolarized. The dependence on handedness of the fermion couplings has enabled SLD to make measurements, using polarized beams, that were in some respects competitive with and complementary to the measurements made at LEP1. (The results quoted in this section are all taken from ref. 12 unless explicitly stated otherwise.)

A number of important electroweak quantities have been determined from measurements around the Z pole at LEP1. The mass of the Z , m_Z , is related to the position of the peak in the cross-section, and total decay width of the Z , Γ_Z , is related to the width of the peak. The accuracy with which $m_Z = (91.1875 \pm 0.0021)$ GeV has been measured is limited by the accuracy with which the mean energy of the colliding beams is known over the entire data-taking period. Achieving such precision was a considerable challenge and resulted from a successful collaboration between physicists from both the LEP experiments and the accelerator. The energy

of a single circulating beam was determined to a high accuracy during dedicated calibrations, using the technique of resonant depolarization. However, such calibrations could be performed only every few days and gave the beam energy only at that specific point in time. The challenge was to propagate this precise knowledge of the beam energy over several days of accelerator running.

The circumference of the beam orbit is fixed by the frequency with which the RF accelerating cavities are excited. This frequency is very stable. The energy of the beams is then determined by the integral around the accelerator ring of the vertical component of the magnetic field experienced by the beams. This vertical magnetic field is produced mainly by the main ‘bending’ dipole magnets, but there is also a contribution from the large number of quadrupole magnets in the machine if the beam is not perfectly centred as it passes through them. If the position of the beam with respect to the quadrupoles changes over a period of hours or days this can affect the beam energy by a significant amount. Lunar tides, high rainfall in the nearby Jura mountains and changes in the water level of Lake Geneva all caused sufficient physical distortion of the accelerator (changing its radius by a few parts in 10^{-9}) to produce a measurable effect on the beam energy.

Erratic electric currents flowing in the accelerator beam pipe also affected the dipole fields over periods of many hours during which beams were circulating in the accelerator. Measurements of the spatial distribution of these currents around the ring established that they were produced by leakage currents from trains running on the Geneva-to-Bellegarde line. Understanding these various effects meant that a model could be developed to predict the beam energy as a function of time during data collection. Ultimately, residual uncertainties in the beam-energy calibration introduced systematic uncertainties of 0.0017 GeV in m_Z and 0.0012 GeV in Γ_Z , correlated among the four experiments.

The total decay width, $\Gamma_Z = (2.4952 \pm 0.0023)$ GeV, is given by the sum of the partial decay widths for each possible type of final-state fermion–antifermion pair. By measuring Γ_Z and the partial decay widths for each

visible final state (quarks and charged leptons), the partial decay width to invisible final states (which in the standard model are neutrino–anti-neutrino pairs) can be determined. This number may be interpreted as a measurement of the number of types of light neutrino produced in Z decay, $N_\nu = 2.9840 \pm 0.0082$. This result requires the measurement of absolute cross-sections. These require a precise determination of the ‘luminosity’ of the accelerator, which is achieved by measuring the rate of low-angle electron–positron scattering. That the necessary precision of order 10^{-4} was achieved in these measurements represents a great success for theorists and experimentalists engaged in this joint project.

The rate of Z decays to quark–antiquark final states is enhanced by a factor related to α_s , the strong coupling constant, $(1 + \alpha_s^2/\pi + \dots)$. Thus, a precise measurement of α_s can be made: $\alpha_s = 0.118 \pm 0.03$. This is in agreement with other precise determinations¹³, such as those from event shapes (which are sensitive to the amount of final-state gluon radiation), and represents an important consistency test of QCD.

Asymmetries

Another class of electroweak measurement made at LEP1 and the SLC is of various asymmetries that are sensitive to the difference between the left- and right-handed couplings. One of the most sensitive of these electroweak measurements, and also one of the easiest to understand, is the so-called left–right asymmetry, A_{LR} . This is measured with polarized e^- beams at the SLC and is defined as:

$$A_{LR} = \frac{\sigma_L - \sigma_R}{\sigma_L + \sigma_R}$$

where σ_L (σ_R) is the cross-section for any given final state with a 100% left-hand (right-hand) polarized incoming electron beam. In practice, 100% polarization is not achievable, but it can be easily shown that if the magnitude of the (luminosity-weighted) average e^- beam polarization is $\langle P_e \rangle$ then the measured asymmetry, A_{LR}^{meas} , is given by $A_{LR}^{\text{meas}} = \langle P_e \rangle A_{LR}$. At the SLC, $\langle P_e \rangle = 70\text{--}80\%$ was regularly achieved.

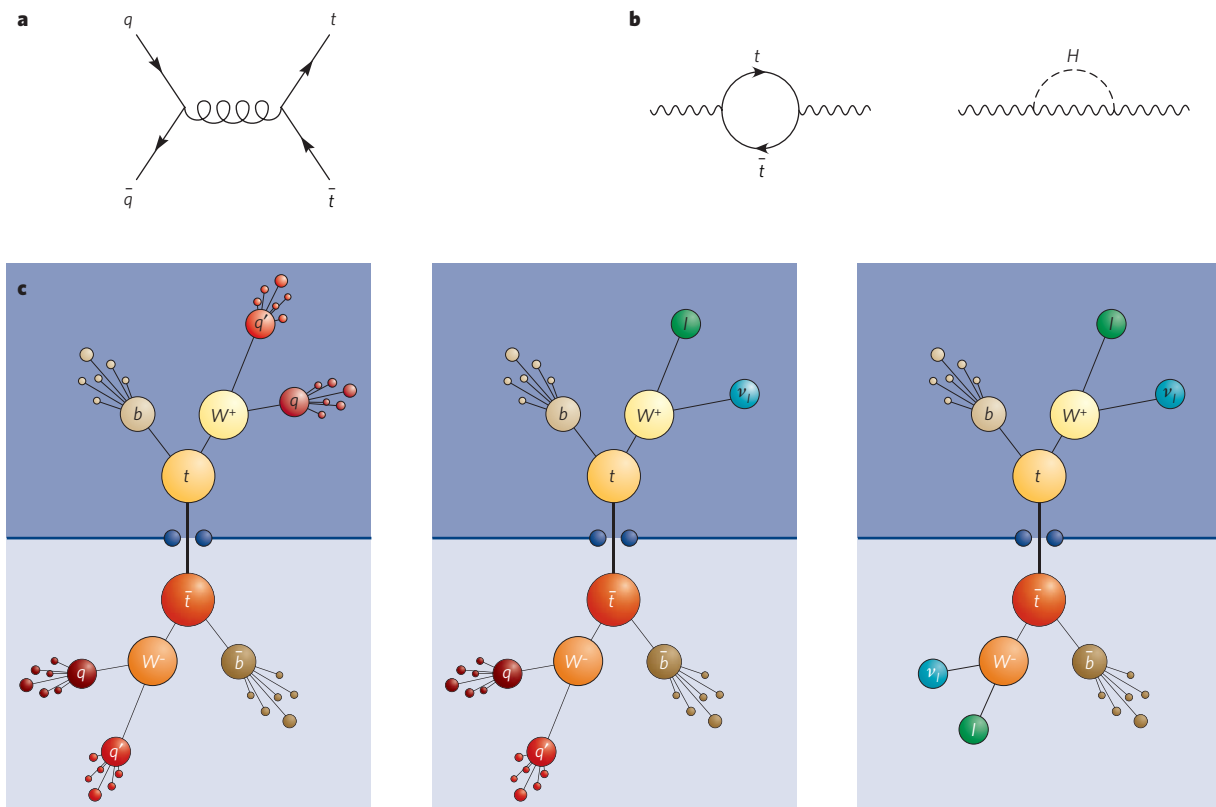


Figure 6 | Top-quark production, and virtual loops. a, The Feynman diagram for $q\bar{q}$ annihilation to produce a $t\bar{t}$ pair. **b,** Virtual loops involving t quarks and Higgs bosons. The left-hand diagram may modify a process involving

the propagation of a photon or Z; the right-hand, the propagation of a W or Z. **c,** The possible event signatures for $t\bar{t}$ production. From left to right, panels show ‘all-jets’, ‘lepton + jets’ and ‘di-lepton’.

The advantage of defining A_{LR} as above is that many factors — such as the dependence on the final-state couplings, acceptance of the detector, and so on — cancel in the ratio (as long as the experimental acceptance and $\langle P_e \rangle$ are independent of the sign of the beam polarization). For such measurements at the Z pole, corrections (which are usually small) must be made to account for the photon-exchange diagram (Fig. 1a) and for the interference between the photon- and Z-exchange diagrams. In addition, a correction has to be applied for the fact that *bremsstrahlung* from the incoming e^+e^- results in an average annihilation centre-of-mass energy that is lower than the nominal E_{cm} of the colliding beams. Results are corrected to correspond to $E_{cm} = m_Z$, and these ‘pole’ cross-sections and asymmetries are therefore to be interpreted as corresponding to pure Z exchange at exactly $E_{cm} = m_Z$; they are sometimes denoted by adding the superscript ‘0’ to the corresponding variable name, for example, A_{LR}^0 .

As we have seen above, the fact that left- and right-handed e^- have different couplings from the Z produces an asymmetry between the annihilation cross-section for left- and right-hand-polarized incoming e^- beams. In addition, the difference between the left- and right-handed fermion couplings produces asymmetries in the angular distributions of the outgoing fermions. Consider an incoming e^- beam that is 100% left-hand polarized: angular-momentum conservation requires that this can annihilate only with the right-handed component of the incoming e^+ beam to produce Zs that are 100% polarized in the direction opposite to the incoming e^- beam. Angular-momentum conservation in the decay of the Z has the consequence that the preferred direction for the outgoing fermions to emerge is along the direction of the incoming e^- beam (the ‘forward’ direction) for left-handed fermions and in the opposite direction (the ‘backward’ direction) for right-handed fermions.

Using polarized electrons, as at the SLC, it is possible to define the ‘left–right forward–backward’ asymmetry,

$$A_{LRFB} \equiv \frac{(\sigma_F - \sigma_B)_L - (\sigma_F - \sigma_B)_R}{(\sigma_F + \sigma_B)_L + (\sigma_F + \sigma_B)_R}$$

As before, the measured asymmetry, A_{LRFB}^{meas} is given by $A_{LRFB}^{meas} = \langle P_e \rangle A_{LRFB}$.

At LEP, the e^- and e^+ beams were unpolarized. That is, there were equal numbers of left- and right-handed incoming beam particles. Nevertheless, the fact that left- and right-handed e^- have different couplings to the Z produces an asymmetry between the numbers of left- and right-hand incoming e^- that annihilate. Thus, the produced Zs are partially polarized along the direction of the incoming beams, and the difference between the left- and right-handed fermion couplings produces a forward–backward asymmetry, A_{FB} , in the angular distributions of the outgoing fermions, which is given by:

$$A_{FB} \equiv \frac{(\sigma_F - \sigma_B)}{(\sigma_F + \sigma_B)}$$

The forward–backward asymmetry with unpolarized beams, A_{FB} , mixes the couplings of the initial- and final-state particles. This makes A_{FB} intrinsically a less sensitive measure of the electroweak mixing angle, θ_W , (in the form $\sin^2\theta_W$) than measurements possible with polarized beams. However, the much larger samples of Zs available at the LEP experiments compensate for this lack of intrinsic sensitivity.

To measure A_{LRFB} and A_{FB} , it is necessary to isolate a sample of Z decays to a particular fermion type and to distinguish the fermion from the antifermion. In the case of Z decays to charged leptons this is fairly straightforward: events containing a high-momentum e^-e^+ , $\mu^-\mu^+$ or $\tau^-\tau^+$ pair may be readily distinguished from one another and from other backgrounds; the electric charge distinguishes the lepton from the antilepton. In the case of Z decays to quarks, precise measurements of A_{FB} are only really possible in the $c\bar{c}$ and $b\bar{b}$ final states.

In most cases it is not possible to determine the handedness of the final-state particles (hence observables are usually summed over this quantity). The one exception is for final-state tau leptons, where the

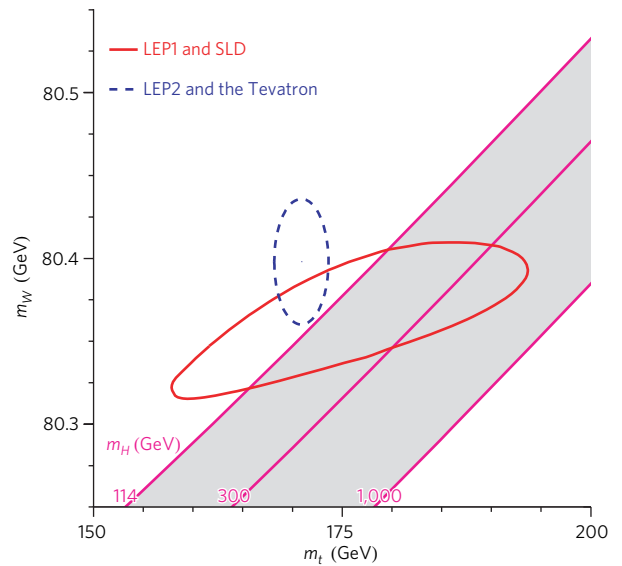


Figure 7 | Contours at 68% confidence level showing the direct (LEP2 and the Tevatron) and indirect (LEP1 and SLD) measurements of m_W and m_t . The shaded band shows the predictions of the standard model for various values of m_H . Figure reproduced, with permission, from ref. 10.

momenta of the observed tau decay products are correlated with the handedness of the produced tau.

All of the asymmetry measurements discussed are sensitive to the difference between the left- and right-handed fermion couplings and thus to the value of $\sin^2\theta_W$. The degree to which the different classes of asymmetry measurements yield consistent values of $\sin^2\theta_W$ — as illustrated in Fig. 4 — represents an important consistency check of the standard model.

Consistency of the standard model

In W^+W^- events at LEP2, the value of m_W is obtained by directly reconstructing the invariant mass of the pair of particles produced in the W decay. In principle, the two final states with high branching ratios — $q\bar{q}l\bar{\nu}$ and $q\bar{q}q\bar{q}$ — give similar statistical sensitivity. However, in the $q\bar{q}q\bar{q}$ channel, uncertainties associated with strong interactions and Bose–Einstein correlations between the products of the two hadronically decaying Ws render the measurement of m_W in this channel less precise. The combination of results¹⁴ from the four LEP experiments yields $m_W = (80.376 \pm 0.033)$ GeV. Other properties of the W (such as the branching ratios shown in Fig. 5) were measured¹⁴ at LEP2.

At the Tevatron, only the leptonic decays $W \rightarrow e\nu$ and $W \rightarrow \mu\nu$ can be used to measure m_W . CDF has produced the first preliminary measurement of m_W using the Run II data accumulated so far, and it has an uncertainty to match that of a single LEP experiment. Including data from Run I, the Tevatron average¹⁰ is $m_W = (80.429 \pm 0.039)$ GeV. Combining the LEP and Tevatron values gives the ‘world average’¹⁰ as $m_W = (80.398 \pm 0.025)$ GeV.

The most important process for producing top quarks in $p\bar{p}$ collisions is shown in Fig. 6a. The dominant decay of the top quark is $t \rightarrow Wb$ and possible signatures of $t\bar{t}$ production are shown schematically in Fig. 6c. If one W decays leptonically and one W decays hadronically, a final state is produced containing a high-transverse-momentum lepton, missing transverse momentum (due to the undetected neutrino) and four high-transverse-momentum jets. This occurs in about 46% of $t\bar{t}$ pairs produced, and this so-called ‘lepton + jets’ channel yields the most precise measurement of m_t . The combination¹⁵ of CDF and DØ measurements gives $m_t = (170.9 \pm 1.8)$ GeV. This precision of around 1% makes m_t by far the most precisely known quark mass. The ultimate precision expected for the Tevatron measurements is around 20 MeV for m_W and around 1 GeV on m_t ; to equal such precision at the LHC will take much time and concerted effort.

It is interesting to understand how experiments can produce evidence for the existence of a particle, and even constrain its mass and couplings,

even though they have insufficient energy to produce the particle directly. The indirect effects of the top quark and the Higgs boson may be observed at LEP/SLC because of the existence of processes such as those shown in Fig. 6b. The possibility of such 'radiative corrections' modifies the simple 'lowest-order' picture of e^+e^- annihilation in Fig. 1a, and experimentally observable effects become sensitive to the masses and couplings of virtual particles in such loops. For example, it is usual to consider $\sin^2\theta_W^{\text{eff}}$, an 'effective' parameter that absorbs the effect of the radiative corrections but allows the basic form of the coupling equations involving $\sin^2\theta_W$ to stay the same. The correction to $\sin^2\theta_W$ can be calculated in the standard model; it depends on the square of the top quark mass, m_t , but only logarithmically on the Higgs mass, m_H . An illustration of these effects is given in the lower half of Fig. 4, in which the experimentally measured value of $\sin^2\theta_W^{\text{eff}}$ is compared with the prediction of the standard model as a function of m_H .

The contours in Fig. 7 show the world-average direct measurements of m_W and m_t , compared with the indirect values of those quantities extracted from the standard-model fit to the LEP and SLC data. The shaded band shows the predictions of the standard model for various values of m_H . The fact that the direct and indirect values of m_W and m_t agree is a triumph of the standard model.

An even more stringent test of the consistency of the standard-model fit to all available high-energy electroweak data is shown in Fig. 8: each measured quantity is compared with its value obtained from the fit. The largest single deviation is seen for $A_{\text{FB}}^{0,b}$ (the forward-backward asymmetry for Z decays to bottom quarks) measured at LEP1, but, particularly given the number of measurements considered, a discrepancy of 2.8 standard deviations in one of them does not meet the threshold required for claiming a significant departure from the standard model.

The increased samples of $t\bar{t}$ events available at Run II have allowed measurements of the cross-section for $t\bar{t}$ production and of t quark properties, such as spin, electric charge and decay branching ratios, that are

consistent with those expected in the standard model¹⁶. The Tevatron experiments are also detecting processes with ever smaller cross-sections— which bodes well for developing the sensitivity of the searches for the Higgs boson at this collider. The CDF experiment has detected the associated production of WZ pairs¹⁷ and has found the first evidence at a hadron collider for the production of ZZ pairs¹⁸; the DØ experiment has found the first evidence for electroweak production of single top quarks¹⁹, enabling the first direct determination of the $t \rightarrow Wb$ coupling.

The years ahead

The next few years will be an exciting time in experimental particle physics, with first collisions at the 14 TeV proton-proton collider, the LHC, scheduled for 2008. Until then, as the world's current highest-energy collider, the Tevatron has a monopoly on direct searches for new physics at a high-mass scale and can perform the most stringent tests of the point-like nature of the fundamental particles.

The Tevatron will run at least until late 2009; its mantle will not pass to the LHC overnight. Except for a few special cases that could produce the most spectacular, unmistakable signatures, it will take time to understand and calibrate the LHC accelerator and detectors.

It is hard to imagine that new physics beyond the standard model will not be found at the LHC. What form that new physics will take is harder to imagine. We know from the past 30 years' work that all theories predicting any observable effects beyond the predictions of the standard model were quickly disposed of by experiment. This means that no matter what is to come, the standard model will remain at least an extremely accurate 'approximation' to the physics of elementary particles at scales up to a few hundred GeV. ■

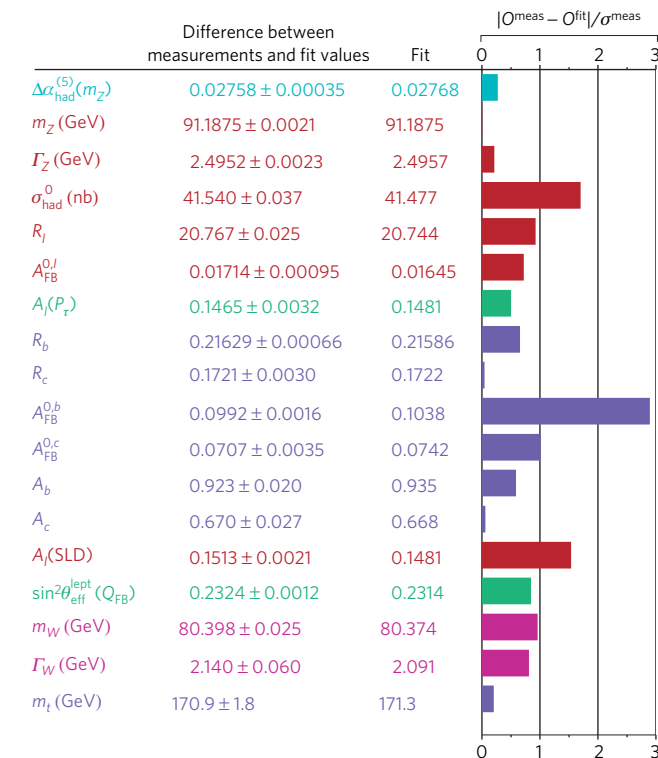


Figure 8 | A test of the consistency of the standard-model fit to all available high-energy electroweak precise data. Each measured observable (O^{meas}) quantity is compared with the value obtained from the fit (O^{fit}). Also shown graphically is the difference between measurement and fit values in number of standard deviations. Colours indicate groups of similar variables. Figure reproduced, with permission, from ref. 10. For full definitions of each quantity, see ref. 10.

1. Arnison, G. *et al.* (UA1 Collaboration). Experimental observation of isolated large transverse energy electrons with associated missing energy at $\sqrt{s} = 540$ GeV. *Phys. Lett. B* **122**, 103–116 (1983).
2. Banner, M. *et al.* (UA2 Collaboration). Observation of single isolated electrons of high transverse momentum in events with missing transverse energy at the CERN $p\bar{p}$ collider. *Phys. Lett. B* **122**, 476–485 (1983).
3. Arnison, G. *et al.* (UA1 Collaboration). Experimental observation of lepton pairs of invariant mass around 95 GeV/ c^2 at the CERN SPS collider. *Phys. Lett. B* **126**, 398–410 (1983).
4. Bagnaia, P. *et al.* (UA2 Collaboration). Evidence for $Z^0 \rightarrow e^+e^-$ at the CERN p collider. *Phys. Lett. B* **129**, 130–140 (1983).
5. Kodama, K. *et al.* (DONUT Collaboration). Observation of tau neutrino interactions. *Phys. Lett. B* **504**, 218–224 (2001).
6. Abachi, S. *et al.* (DØ Collaboration). Top quark search with the DØ 1992–1993 data sample. *Phys. Rev. D* **52**, 4877–4919 (1995).
7. Abachi, S. *et al.* (DØ Collaboration). Search for the top quark in $p\bar{p}$ collisions at $\sqrt{s} = 1.8$ TeV. *Phys. Rev. Lett.* **72**, 2138–2142 (1994).
8. Abe, F. *et al.* (CDF Collaboration). Observation of top quark production in $p\bar{p}$ collisions with the collider detector at Fermilab. *Phys. Rev. Lett.* **74**, 2626–2631 (1995).
9. Abachi, S. *et al.* (DØ Collaboration). Observation of the top quark. *Phys. Rev. Lett.* **74**, 2632–2637 (1995).
10. LEP Electroweak Working Group. *LEP Electroweak Working Group*. <<http://lepewwg.web.cern.ch/LEPEWWG/>> (2007).
11. ALEPH Collaboration, DELPHI Collaborations, L3 Collaboration, OPAL Collaboration and The LEP Working Group for Higgs Boson Searches. Search for the standard model Higgs boson at LEP. *Phys. Lett. B* **565**, 61–75 (2003).
12. ALEPH, DELPHI, L3, OPAL, SLD collaborations, LEP Electroweak Working Group, the SLD Electroweak and Heavy Flavour Groups. Precision electroweak measurements on the Z resonance. *Phys. Rep.* **427**, 257–454 (2006).
13. Jones, R. W. L. Final α_s combinations from the LEP QCD working group. *Nucl. Phys. B Proc. (suppl.)* **152**, 15–22 (2006).
14. The LEP Collaborations: ALEPH Collaboration, DELPHI Collaboration, L3 Collaboration, OPAL Collaboration, the LEP Electroweak Working Group. A combination of preliminary electroweak measurements and constraints on the standard model. Preprint at <<http://arxiv.org/abs/hep-ex/0612034>> (2006).
15. Tevatron Electroweak Working Group (for the CDF and DØ Collaborations). A combination of CDF and DØ results on the mass of the top quark. Preprint at <<http://arxiv.org/abs/hep-ex/0703034v1>> (2007).
16. Quadt, A. Top quark physics at hadron colliders. *Eur. Phys. J. C* **48**, 835–1000 (2006).
17. Abulencia, A. *et al.* (CDF Collaboration). Observation of WZ production. Preprint at <<http://arxiv.org/abs/hep-ex/0702027>>.
18. CDF Collaboration. Evidence for ZZ production in $p\bar{p}$ at $\sqrt{s} = 1.96$ TeV. CDF Note 8775 (preliminary). <http://cdcfwww.fnal.gov/physics/ewk/2007/ZZ/ZZ_comb_public_note.ps>.
19. Abazov, V. M. *et al.* (DØ Collaboration). Evidence for production of single top quarks and first direct measurement of $|V_{tb}|$. *Phys. Rev. Lett.* **98**, 181802 (2007).

Author information Reprints and permissions information is available at npg.nature.com/reprintsandpermissions. The author declares no competing financial interests. Correspondence should be addressed to T.W. (twyatt@fnal.gov; Terry.Wyatt@manchester.ac.uk).